Monthly Notices of the ROYAL ASTRONOMICAL SOCIETY

MNRAS **548,** 1–12 (2026) https://doi.org/10.1093/mnras/stag665
Advance Access publication 2026 April 9

Twenty-four thousand hours of GREENBURST observations with the GBT

J. W. Kania [1,2,3] S. Paine,[1,2] G. M. Doskoch [1,2] S. Tabassum,[1,2] S. Sirota,[1,2] M. Flanagan,[1,2] K. Halley,[1,2] D. R. Lorimer [1,2★] E. Mayfield,[4] M. A. McLaughlin [1,2] E. Fonseca,[1,2] D. Agarwal [1,2] M. P. Surnis,[5] F. Crawford [6] T. Jespersen,[6] E. Craver,[6] M. Golden,[6] A. Turan,[6] J. Muyskens,[6] D. Adair,[6] Fengqiu Adam Dong,[7,8] A. P. V. Siemion,[3,9,10,11] G. Golpayegani,[1,2] M. B. Mickaliger,[3] K. M. Rajwade [9] and I. H. Stairs[12]

[1]*Department of Physics and Astronomy, West Virginia University, Morgantown, WV 26506-6315, USA*
[2]*Center for Gravitational Waves and Cosmology, Chestnut Ridge Building, Morgantown, WV 26505-6315, USA*
[3]*Jodrell Bank Centre for Astrophysics, University of Manchester, Alan Turing Building, Oxford Road M13 9PY, UK*
[4]*Department of Physics and Astronomy, Appalachian State University, Boone, NC 28608-2106, USA*
[5]*Department of Physics, IISER Bhopal, Bhauri Bypass Road, Bhopal 462066, India*
[6]*Department of Physics and Astronomy, Franklin and Marshall College, P.O. Box 3003, Lancaster, PA 17604, USA*
[7]*National Radio Astronomy Observatory, 520 Edgemont Rd, Charlottesville, VA 22903, USA*
[8]*Green Bank Observatory, 155 Observatory Road, Green Bank, WV 24944, USA*
[9]*Sub-Department of Astrophysics, Department of Physics, University of Oxford, Parks Rd, Oxford OX1 3PU, UK*
[10]*SETI Institute, 339 N. Bernardo Ave, Mountain View, California 94043, USA*
[11]*Berkeley SETI Research Center, University of California, 339 Campbell Hall, Berkeley, CA 94720, USA*
[12]*Department of Physics and Astronomy, University of British Columbia, 6224 Agricultural Road, Vancouver, BC V6T 1Z1, Canada*

Accepted 2026 April 2. Received 2026 March 19; in original form 2026 January 27

ABSTRACT

In addition to fast radio burst (FRB) searches carried out using dedicated surveys, a number of radio observatories take advantage of commensal opportunities with large facilities in which observations for other projects can be searched for FRBs and other transient sources. We present the results from one such effort, the first 24 186 h of the GREENBURST search for dispersed radio pulses with the Green Bank Telescope (GBT). To date, GREENBURST has detected a total of 50 pulsars and three FRBs. One of the pulsars, PSR J0039+5407, has a period of 2.2 s and was previously unknown. Using follow-up observations with the Canadian Hydrogen Intensity Mapping Experiment, we found a timing solution for this pulsar which shows it to have a characteristic age of 2 Myr. Additional GBT observations show the pulsar has a very high nulling fraction (∼70–80 per cent). All three of the FRBs are repeating sources that were previously known and were being monitored by the GBT as part of other projects. A major challenge for GREENBURST in the discovery of new FRBs is its single beam. This makes it hard to distinguish some of the pulses from sources of radio frequency interference. We highlight this problem with a case study of an FRB-like pulse that initially passed our interference filters. Upon closer inspection, the event appears to be part of a longer duration narrow-band source of unknown origin. Further observations and monitoring are required to determine whether it is terrestrial or celestial.

Key words: methods: observational – pulsars: general – pulsars: individual: PSR J0039+5407 – fast radio bursts.

1 INTRODUCTION

As a population of cosmological sources of unknown origin, fast radio bursts (FRBs) are insightful probes of fundamental physics and the large-scale structure of the Universe (for a recent review, see B. Zhang 2023). Among the many (for a living compilation, see E. Platts et al. 2019) possible sources suggested to explain FRBs so far are extragalactic magnetars and compact object mergers. The discovery of repeating FRBs (L. G. Spitler et al. 2016; CHIME/FRB Collaboration 2019) suggests that at least some FRBs are produced in non-catastrophic events. The discovery of FRB-like emission from the Galactic magnetar SGR 1953+2154 (C. D. Bochenek et al. 2020; CHIME/FRB Collaboration 2020) provides strong evidence in favour of a magnetar origin for some fraction of the FRB population. The discoveries of FRBs in galaxies at increasingly larger redshifts (S. D. Ryder et al. 2023; M. Caleb et al. 2025) highlight the need to characterize this population using high-sensitivity instruments.

★ E-mail: duncan.lorimer@mail.wvu.edu

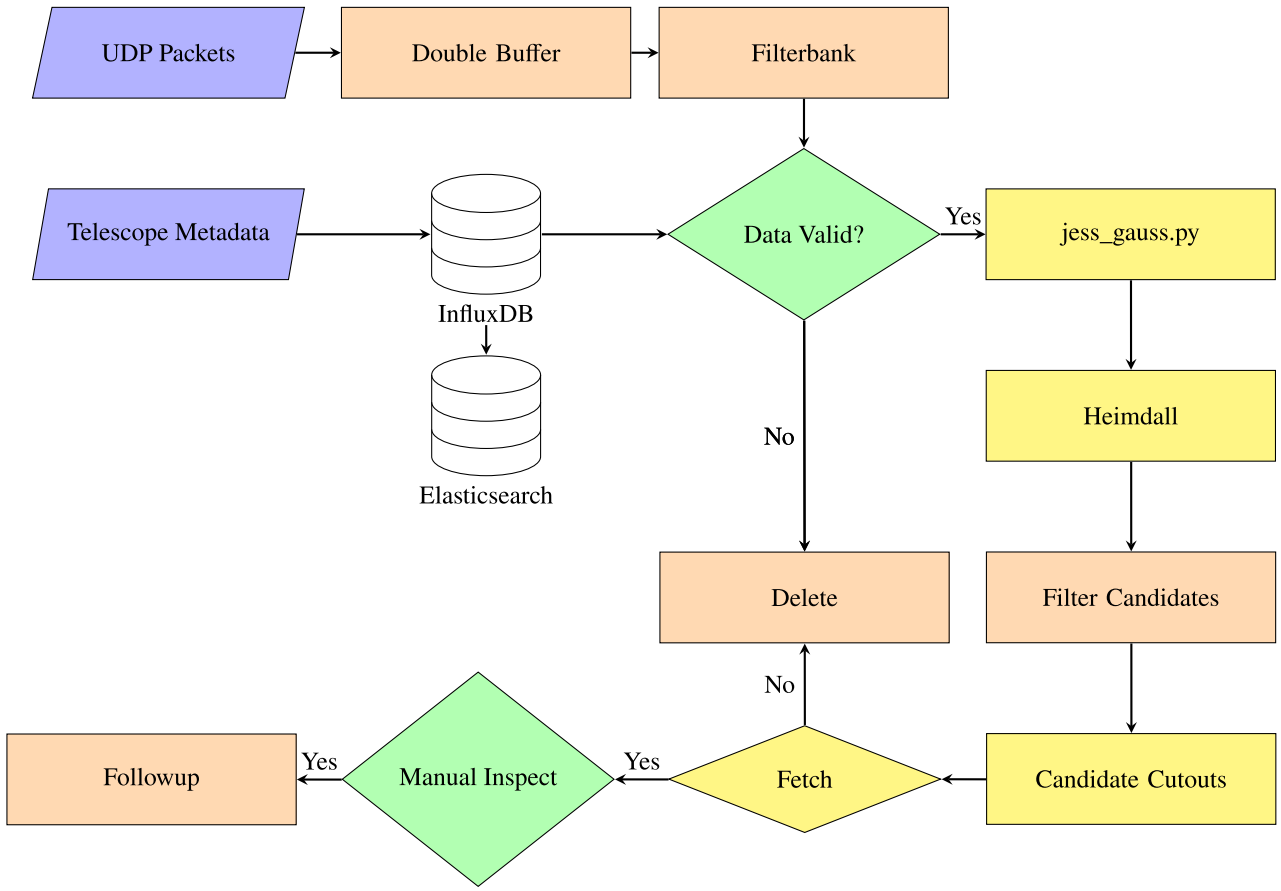

Figure 1. Schematic showing the GREENBURST data acquisition and analysis pipeline. The blue input squares are data provided by the Serendip VI (K. Archer et al. 2016) backend. Data are sent to GREENBURST via UDP packets which are buffered and written in `filterbank` format (D. R. Lorimer 2011). The double buffer ensures continuous data coverage over discrete filterbanks. The Elasticsearch data base keeps track of the telescope pointing at 8 min cadence over the lifetime of the experiment. If the data are valid (suitable receiver position, not in maintenance, etc.) they are cleaned with JESS_GAUSS.PY's Jarque-Bera filter. These cleaned filterbank data are subsequently searched with `heimdall` (B. R. Barsdell 2012). Candidate pulses are cut out and classified as astrophysical or RFI by FETCH (D. Agarwal et al. 2020b). Candidates classified as astrophysical are reviewed by humans on a daily basis via a dedicated `Slack` channel. An InfluxDB2 keeps track of the telescope pointing at a cadence of 1 s. Yellow squares show steps that leverage GPU acceleration.

Motivated by the need to find more FRBs, as part of a collaboration with groups engaged in the search for extraterrestrial intelligence (J. Chennamangalam et al. 2017) using the SERENDIP VI backend architecture (K. Archer et al. 2016), we began building and commissioning real-time commensal FRB detectors on the Arecibo (ALFABURST; G. Foster et al. 2018a) and Green Bank (GREENBURST; M. P. Surnis et al. 2019) telescopes. Since the demise of the Arecibo telescope, our focus has been on GREENBURST, with commissioning and initial observations being reported by D. Agarwal et al. (2020a). A key component of that work was our development (D. Agarwal et al. 2020b) of the Fast Extragalactic Transient Candidate Hunter (FETCH), a deep-learning model that autonomously identifies FRBs. Some of the development of FETCH, particularly in the form of early training data, was provided by GREENBURST commissioning observations.

The goal of GREENBURST is to detect dispersed radio pulses of astrophysical origin by piggybacking on Green Bank Telescope (GBT) observations. Since 2019, GREENBURST has collected over 20 000 h of GBT data as part of its routine operations, increasing the scientific productivity of the telescope and providing a basis for PhD projects (D. Agarwal 2020; G. Golpayegani 2020; J. W. Kania 2023). We describe these observations in this work which has so far led to the successful detections of FRBs and pulsars as well as the discovery of one Galactic pulsar through the detection of individual pulses.

The plan for the rest of this paper is as follows. In Section 2, we briefly describe the observational framework of GREENBURST as well as infrastructure developments made since the description provided by D. Agarwal et al. (2020a). In Section 3, we detail our main results to date. The implications of these results are discussed further in Section 4 before we conclude with some projections for the future in Section 5.

2 OBSERVATIONAL OVERVIEW AND UPDATES

As described in detail in M. P. Surnis et al. (2019), GREENBURST and SERENDIP VI (K. Archer et al. 2016) share a copy of the signal from the L band (1.4 GHz) feed from the GBT. A schematic of the resulting data flow and analysis pipeline

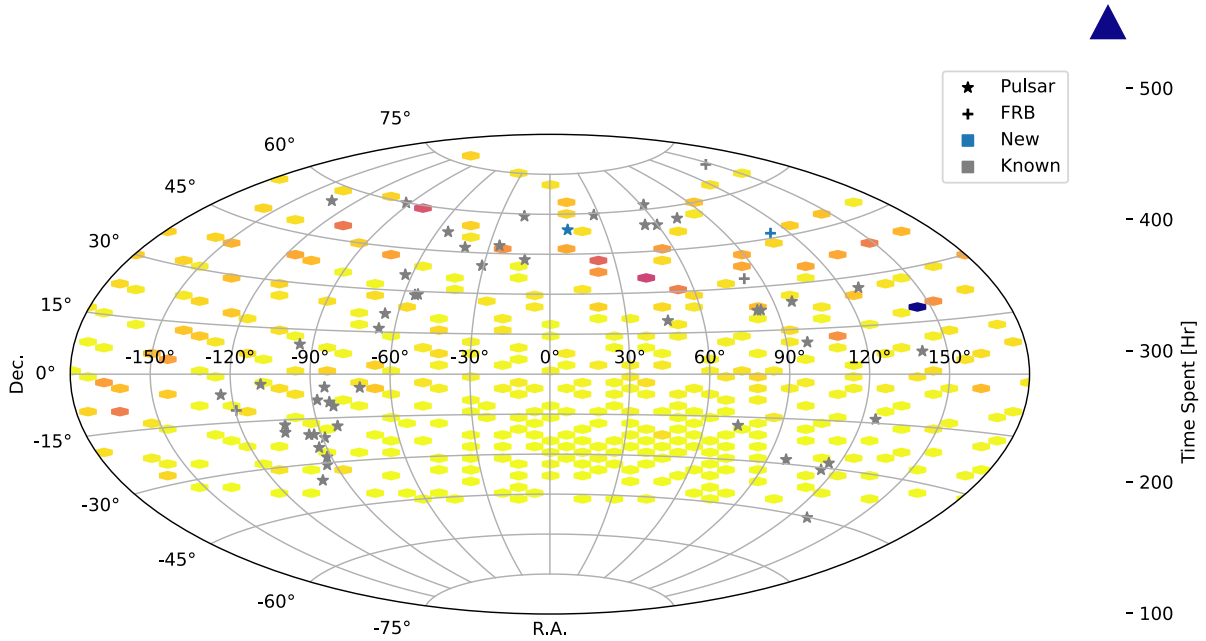

Figure 2. Sky coverage for the observation period reported in this paper. The positions are quantized into 6 deg^2 hexagons and colour coded into hours spent per region. Stars indicate pulsars, crosses indicate FRBs. Grey points are known objects. The blue star is represents PSR J0039+5407. The blue cross is GBP 220718.

is shown in Fig. 1. The GREENBURST signal is 4096 channels covering 960 MHz, centred at 1440 MHz sampled at 256 μs with 8-bit precision. These data are searched for the presence of dispersed pulses of astrophysical origin with a pipeline optimized for the detection of pulses with dispersion measures (DMs) from 10 to 10 000 pc cm^{-3} and widths from 256 μs to 32.8 ms. Further details of the data analysis pipeline can be found in D. Agarwal et al. (2020a). The major change to the pipeline since this earlier account has been the implementation (J. W. Kania 2023) of more sophisticated techniques to remove unwanted radio frequency interference (RFI) signals, as described below.

Radiometer noise and signals from astronomical sources are expected to be normally distributed (G. M. Nita et al. 2007; G. M. Nita & D. E. Gary 2010). Communication systems are non-thermal, and therefore are often highly non-Gaussian, and we expect communication signals, one of the main sources of RFI, to have higher statistical moments (M. Rafiei-Ravandi & K. M. Smith 2023). We therefore use normality tests to discriminate between astrophysical and anthropogenic signals. Spectral kurtosis (the fourth normalized moment) has been shown to be an excellent discriminator for RFI, and subject of much development by the radio astronomy community (G. M. Nita et al. 2007; D. E. Gary, Z. Liu & G. M. Nita 2010; G. M. Nita & D. E. Gary 2010; G. M. Nita, A. Keimpema & Z. Paragi 2019; J. Taylor et al. 2019; A. Mirhosseini 2020; E. Smith, R. S. Lynch & D. J. Pisano 2022). Kurtosis measures the tails of a distribution, making it insensitive to signals with a 50 per cent duty cycle. This insensitivity has traditionally been mitigated by using multiscale kurtosis tests (D. E. Gary et al. 2010; E. Smith et al. 2022).

As will be described in detail in an upcoming paper (Kania et al. in preparation), we investigated alternative normality tests which involve both kurtosis and skew (third normalized moment). For this paper, we look for outliers in kurtosis and skew individually, then combine the resulting masks. We look for outliers in the Jarque–Bera statistic (C. M. Jarque & A. K. Bera 1980; A. K. Bera & C. M. Jarque 1981; C. M. Jarque & A. K. Bera 1987) or D'Agostino's K^2 statistic (R. D'Agostino & E. S. Pearson 1973; R. B. D'Agostino & A. Belanger 1990). Outliers are identified by calculating the inter-quartile range (IQR) and flagging samples that are four standard deviations away from the median. IQR is a robust measure of scale (P. Rousseeuw & C. Croux 1992; V. Morello, K. M. Rajwade & B. W. Stappers 2022), making it resilient to RFI-contaminated sections of spectra. We consider blocks of 64 and 4096 samples (corresponding to approximately 16 ms and 1 s, respectively). Additionally, following the normality-based excision, we flag sections on a 16 384 sample (4.2 s) cadence with unusually high median versus mean absolute difference. While we expect RFI to be more prominent at higher moments, some RFI seems to be particularity strong driving the signal chain into a non-linear state. These non-linear sections do not show up more significantly at higher statistical moments, so we perform this first-moment normality test. Once we have excised sections of dynamic spectra based on their normality, we use the high-pass filter first described in R. P. Eatough, E. F. Keane & A. G. Lyne (2009) and further refined by P. Lazarus et al. (2015). R. P. Eatough et al. (2009) describes a technique to remove broad-band signals by taking the mean across all frequency channels, creating a zero-DM time series then subtracting this time series from each frequency channel. This works well when there is uniform frequency response. Often, telescopes do not have uniform sensitivity across their bandpass, due to receiver roll-off and band-stop filter. To overcome this changing sensitivity, P. Lazarus et al. (2015) introduce a weighted zero-DM subtraction technique that uses the bandpass shape to account for this changing receiver sensitivity by using a weighted bandpass. As described in (J. W. Kania et al. 2026), we use this technique to remove broad-band RFI in addition to the noise diode.

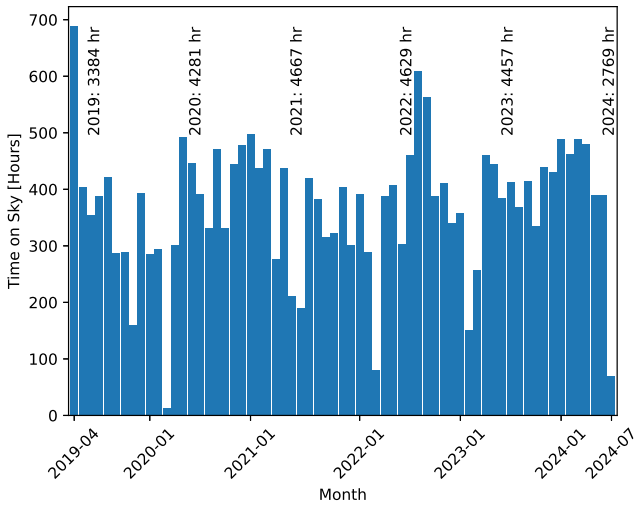

Figure 3. Timeline of observation showing totals for each year. The 2024 total is up to the end of July. Overall, the *L*-band receiver was in focus 72 per cent of the time. Other receivers being used by the primary observer were: *X* band 12 per cent, *C* band 7 per cent, Ka band 5 per cent and Mustang 3 per cent.

3 RESULTS

The results from this work cover GBT observations between 2019 March 14 and 2024 July 31 during which time a total of 24 186 h of data were collected. Fig. 2 shows an equatorial projection of the sky coverage to date. Fig. 3 shows the time spent on sky as a function of epoch. In the subsections below, we detail the main outcomes.

3.1 Detections of previously known sources

Our observations to date have resulted in the detection of 16 556 pulses from 49 previously known pulsars. These detections are summarized in Table 1 and the brightest pulse from each source is shown in Fig. 4. While further analyses of these pulses will be provided in a subsequent publication (Tabassum et al. in preparation), some notable detections among this sample are: bright pulses from the 11 ms pulsar B1744–24A in Terzan 5 (which are characterized in earlier GBT observations by A. V. Bilous, S. M. Ransom & P. Demorest 2019, and thought to be due to plasma lensing in this eclipsing binary system), giant pulses from the first millisecond pulsar B1937+21 (I. Cognard et al. 1996), and individual pulses from the 22.7 ms pulsar J0737–3039A in the double pulsar system (M. Burgay et al. 2003; A. G. Lyne et al. 2004).

3.2 Previously known FRBs

During the observing period reported here, three repeating FRBs were observed by the GBT for which we have detections: FRB 20190520B (C. H. Niu et al. 2022) was observed as part of project GBT20B_401, FRB 20200120E (M. Bhardwaj et al. 2021) was observed as part of project GBT22A_502, and FRB 20121102A (L. G. Spitler et al. 2016) was observed as part of project GBT21A_417. Sample pulses from these sources are shown in Fig. 5. As these data were collected for other projects with specific scientific goals, we do not use them for any purposes beyond their value as a test of the ability of our data analysis pipeline to make serendipitous detections of FRB pulses.

Table 1. The 49 previously known pulsars detected during GREENBURST operations. For each pulsar, we list the spin period (P), DM, 1400 MHz flux density (S_{1400}), number of epochs ($N_{\rm epochs}$) on which the source was detected, and the total number of pulses detected ($N_{\rm pulses}$).

PSR	P (ms)	DM (cm^{-3} pc)	S_{1400} (mJy)	$N_{\rm epochs}$	$N_{\rm pulses}$
B0144+59	196.32	40.1	2.1	1	4
B0301+19	1387.58	15.7	15.0	3	4
B0329+54	714.52	26.8	203.0	31	837
B0355+54	156.38	57.1	23.0	96	4408
B0402+61	594.58	65.4	2.8	1	17
B0450−18	548.94	39.9	17.0	2	557
B0450+55	340.73	14.6	13.0	1	1
B0525+21	3745.54	50.9	8.9	3	13
B0531+21	33.39	56.8	14.0	1	1
B0626+24	476.62	84.2	3.2	5	107
B0628−28	1244.42	34.4	32.0	1	91
J0631+1036	287.82	125.3	1.1	1	10
J0737−3039A	22.69	48.9	1.3	2	3
B0740−28	166.76	73.7	26.0	14	314
B0818−13	1238.13	40.9	6.0	3	169
B0823+26	530.66	19.5	10.0	1	164
B0833−45	89.33	67.8	1050.0	1	146
B0919+06	430.63	27.3	10.0	1	32
B1508+55	739.68	19.6	8.0	5	44
B1540−06	709.06	18.3	2.0	1	110
B1642−03	387.69	35.8	25.8	1	338
B1702−19	298.99	22.9	5.7	52	4189
B1706−16	653.05	24.9	15.0	1	162
B1718−35	280.42	496.8	16.8	4	540
J1740+1000	154.10	23.9	2.7	1	2
J1741−2019	3904.51	74.9	0.0	2	2
B1742−30	367.43	88.4	21.0	3	66
B1745−20A	288.60	219.4	0.4	1	2
B1744−24A	11.56	242.2	0.6	3	13
J1749+5952	436.04	45.1	0.0	1	1
B1749−28	562.56	50.4	48.0	3	3
B1800−21	133.67	234.0	9.6	1	8
B1804−08	163.73	112.4	18.0	2	108
B1818−04	598.08	84.4	10.1	1	18
B1822−09	769.02	19.4	10.0	3	6
B1826−17	307.13	216.8	11.0	1	3
B1828−11	405.07	159.7	1.5	15	1216
B1911−04	825.94	89.4	6.8	1	53
B1933+16	358.74	158.5	58.0	15	1001
B1937+21	1.56	71.0	13.9	21	33
B1946+35	717.31	129.4	8.3	4	98
B2016+28	557.95	14.2	30.0	1	5
B2020+28	343.40	24.6	38.0	6	640
B2021+51	529.20	22.6	27.0	36	828
B2111+46	1014.69	141.2	19.0	1	4
B2154+40	1525.27	71.1	17.0	1	21
B2217+47	538.47	43.4	3.0	2	67
B2255+58	368.25	151.1	9.2	1	39
B2310+42	349.43	17.3	15.0	4	61

3.3 PSR J0039+5407

On 2022 June at 10:14:34 UTC, we detected a pulse with a signal-to-noise ratio (S/N) of 14 and a DM of 74.2 cm^{-3} pc. Upon RFI cleaning using the composite filter in JESS (J. W. Kania et al. 2026), eight additional lower-significance pulses were detected.

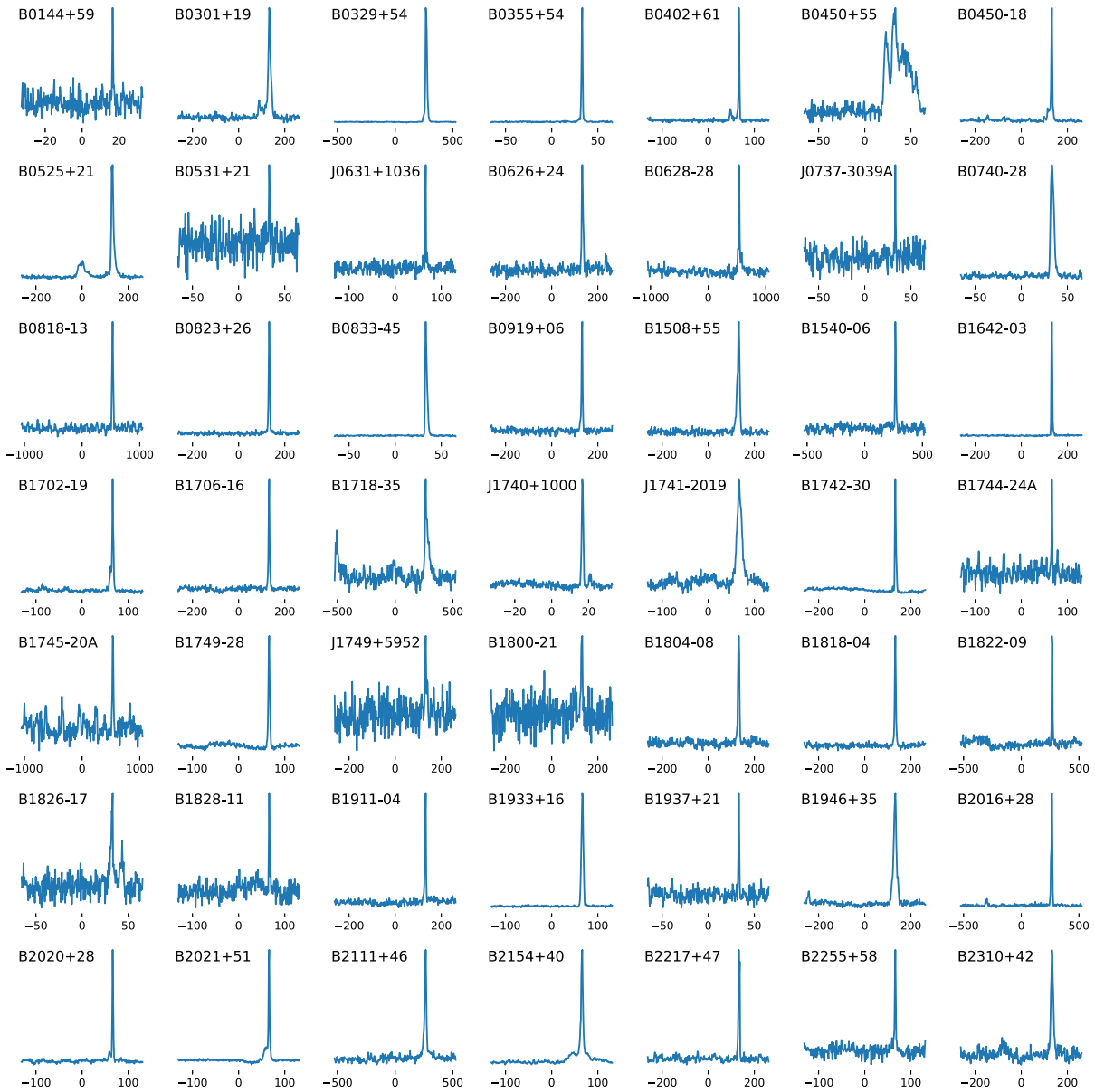

Figure 4. Sample individual pulses detected from the 49 pulsars in Table 1. The numerical labels under each pulse denote time in ms with respect to the centre of the time series. For presentation purposes, each pulse has been aligned so that its peak value is located 75 per cent along the horizontal axis.

The initial pulse was found again at S/N = 29, corresponding to a peak flux density of about 70 mJy, as well as three additional pulses in the 10–30 mJy range. Manual inspection of candidates with DMs around 70 cm^{-3} pc revealed another five pulses during the time the pulsar was drifting through the telescope's field of view. From these nine pulses, we were able to determine the most probable position of the pulsar and identify its period. Using a kernel density estimation (KDE; M. Rosenblatt 1956; E. Parzen 1962) approach, the most probable position of the pulsar was found. As input to the KDE process, we used a Gaussian smoothing kernel that has a width equal to the telescope beam, (9.2 arcmin; M. P. Surnis et al. 2019). We then used the S/N of the detected pulses as relative weights for the kernels using scikit-learn's KDE implementation (F. Pedregosa et al. 2011). This yielded an initial estimate of the right ascension (J2000) consistent with a point source drifting through the beam. The declination uncertainty is simply the width of the telescope beam. A standard Fourier transform-based search for periodicities in these data using PRESTO (S. Ransom 2011) did not reveal any significant candidates. A fast folding algorithm search using `riptide` (V. Morello et al. 2020), however, revealed the presence of a 2.2 s periodicity consistent with the presence of a radio pulsar with that period. These initial parameters were subsequently refined during the follow-up timing analysis for the pulsar (henceforth referred to as PSR J0039+5407) described in Section 4.1.

3.4 GBP 20220718

On 2022 July 18 at 16:07:17 UTC, we detected a pulse of width 16 ms with a DM of 145.5 cm^{-3} pc and S/N of 10. From the position of the telescope at the time of detection, we estimate the

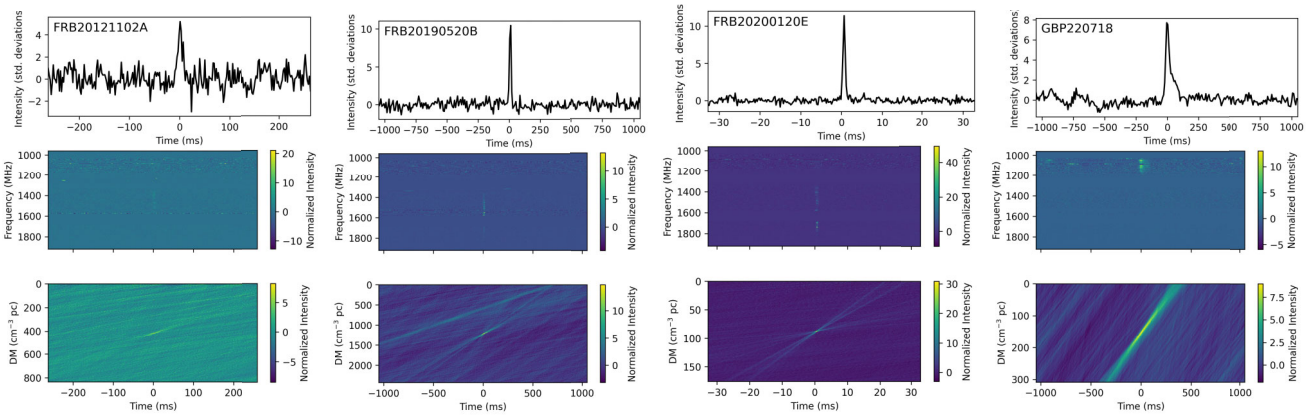

Figure 5. Example detections of individual pulses from the three previously known FRBs (FRB 20121102A, FRB 20190520B, and FRB 20200120E) observed during follow-up observations of these sources as well as the discovery pulse for GBP 220718. In each case the top panel shows the dedispersed pulse, the middle panel shows the 'waterfall' plot of frequency versus time, while the bottom panel shows the trial DM as a function of time. In each of the data visualizations, the median has been subtracted from the data and the resulting arrays have been divided by their respective standard deviation.

right ascension to be $07^{h}\ 25^{m}\ 13^{s} \pm 18^{s}$ and the declination to be $+46^{\circ}\ 31.8' \pm 4.5'$. As shown in the discovery plot in Fig. 5, the signal was limited to the lower quarter of the bandpass. In our discussion below, due to additional emission that we subsequently found in the original observation, we do not feel confident in currently concluding that it is celestial in origin and henceforth refer to it as GBP 220718, where GBP stands for GREENBURST pulse.

4 DISCUSSION

In the following sections, we discuss the findings from follow-up observations of both PSR J0039+5407 and GBP 220718.

4.1 PSR J0039+5407

Starting from the initial measurements of the period, DM and position obtained from the discovery observations presented above we carried out regular observations of this pulsar using CHIME/Pulsar (CHIME/Pulsar Collaboration 2021). Using a preliminary ephemeris for this pulsar made from initial CHIME/FRB (CHIME/FRB Collaboration 2018) observations in search mode in July 2022, a further 134 timing mode observations of 1430 s were taken by CHIME between 2022 August 16 and 2024 March 6. Carrying out a standard timing analysis using the TEMPO2 software package (G. B. Hobbs, R. T. Edwards & R. N. Manchester 2006) yields a phase-connected solution spanning 446 d with parameters summarized in Table 2. The integrated profile obtained by summing all of the CHIME/PSR observations is shown in Fig. 6. The DM fit to the TOAs was carried out by generating eight 50 MHz sub-bands from one of the strongest CHIME/Pulsar detections and keeping the other parameters in the solution fixed.

4.1.1 *Nulling analysis*

Some pulsars exhibit nulling, a pattern of intermittent intervals during which the pulsar enters a state of minimal to no emission (D. C. Backer 1970). Nulling can occur on a wide variety of time-scales (N. Wang, R. N. Manchester & S. Johnston 2007),

Table 2. Observed and derived parameters for PSR J0039+5407. The distance parameters were derived using the NE2025 model (S. K. Ocker & J. M. Cordes 2026).

Parameter	Value
Right ascension, α (h:m:s) (J2000)	00:39:11.65(2)
Declination, δ (deg:m:s) (J2000)	54:07:11.6(1)
Spin frequency, ν (Hz)	0.446192165098(9)
Spin frequency derivative $\dot{\nu}$ (s^{-2})	$-3.12(1)\times10^{-15}$
Epoch of period (MJD)	60 102
DM (cm^{-3} pc)	72.9(1)
Galactic longitude, l (deg)	121.12
Galactic latitude, b (deg)	–8.71
50 per cent pulse width, w_{50} (ms)	64
10 per cent pulse width, w_{10} (ms)	92
DM-derived distance, d (kpc)	3.0
Height above the Galactic plane, z (pc)	450
Characteristic age, τ (Myr)	2.3
Magnetic field strength, B (10^8 T)	6.0
Spin-down luminosity, $\dot{E}$ (10^{24} W)	5.5

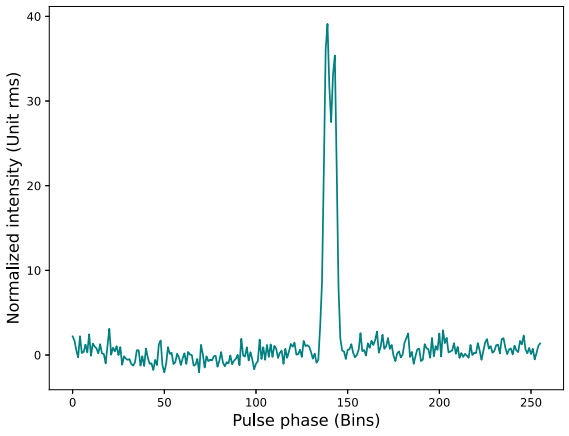

Figure 6. Composite profile of J0039+5407 from the phase-coherent addition of the best CHIME/Pulsar detections. The total integration time is 4263 s.

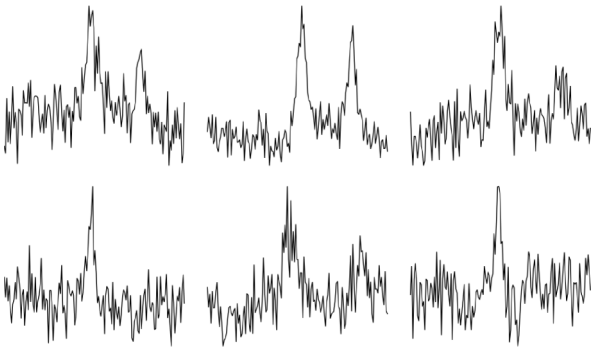

Figure 7. Six single pulses from a GBT 820 MHz observation of J0039+5407 exhibiting several types of morphology. Some pulses show only one peak while others show both. The trailing peak of multicomponent pulses is weaker. The horizontal extent of each of the pulses shown is 100 ms and the time series has been downsampled by a factor of 16.

depending on the pulsar. Previous studies have reported correlations between the fraction of null pulses (the null fraction, NF) and pulse period P (J. D. Biggs 1992) and characteristic age τ (R. T. Ritchings 1976; N. Wang et al. 2007), with the latter relationship being even stronger. With $P \simeq 2.24$ s and $\tau \simeq 2.3$ Myr, it would not be surprising if PSR J0039+5407 exhibited nulling.

We conducted an analysis to find NF for PSR J0039+5407 using a GBT observation of the pulsar carried out at a central frequency of 820 MHz using the VEGAS spectrometer (R. M. Prestage et al. 2015) in search mode using 2048 channels over a total bandwidth of 200 MHz sampled every 80 μs. Using the timing solution, we folded the data into single pulses. Fig. 7 shows a selection of the strongest single pulses. An examination of the folded profile showed that the majority of emission is concentrated within a span of ∼0.1 s, which we designate the on-pulse region. Following the method of P. R. Brook, A. Karastergiou & S. Johnston (2019), after subtracting a baseline from each pulse, we summed the time series over the on-pulse region, yielding some fluence F. For the purposes of the analysis below, the fluence scale does not require calibration. However, from radiometer noise considerations (see, e.g. D. R. Lorimer & M. Kramer 2004), we find typical peak flux densities on the order of 1 Jy in this observing band (720–920 MHz).

Assuming Gaussian noise, the pulse periods from nulling should yield fluences following a Gaussian distribution centred at $F = 0$. The pulse periods with strong single-pulse emission, on the other hand, should follow a lognormal distribution (S. Burke-Spolaor et al. 2012).[1] We can compute the nulling fraction by fitting a sum of a Gaussian (centred at $F/\langle F\rangle = 0$) and lognormal distribution to the empirical flux density histogram. If the two component distributions have fitted amplitudes A_n and A_e, respectively, then

$$\mathrm{NF} = \frac{A_\mathrm{n}}{A_\mathrm{n} + A_\mathrm{e}}, \tag{1}$$

where we have ensured that each distribution, before fitting, was normalized to have unit area; in other words, A_n and A_e are also the areas under the distributions. We performed the fits using

[1]While some pulsars follow a slightly different distribution (M. B. Mickaliger et al. 2018), a lognormal approximation should be sufficient for our purposes.

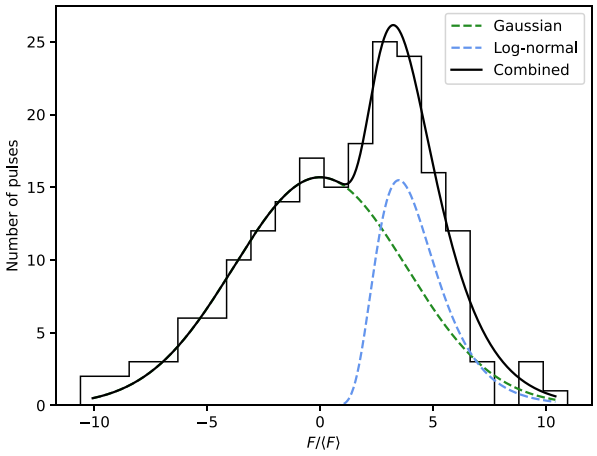

Figure 8. Histograms of normalized single-pulse fluences of J0039+5407, along with the two-component fits. The Gaussian is centred at zero and represents spin periods dominated by noise (the nulls) while the lognormal distribution represents spin periods with stronger emission.

the `optimize.curve_fit` routine from the SCIPY[2] package (P. Virtanen et al. 2020). The fitted histograms are shown in Fig. 8, and yielded NF = 73 ± 3 per cent, where the uncertainty in NF was found by propagating the uncertainties in A_n and A_e in quadrature.

We checked this value of NF using the earlier method of R. T. Ritchings (1976), who generated histograms of fluence from the on-pulse region and a subset of the off-pulse region, and computed the scaling factor required to make the two comparable; they identify this scaling factor with the nulling fraction. This results in a NF = 80 ± 7 per cent, consistent with the value found above. Further observations of this pulsar to obtain high-quality pulse sequences to better characterize the single-pulse behaviour are strongly encouraged.

4.2 GBP 220718

4.2.1 Search for low earth orbiting spacecraft

As the number of low-Earth orbit (LEO) satellites continues to increase (J. C. McDowell 2020), distinguishing between transient RFI and genuine astrophysical signals has become vital. Indeed, a very narrow (ns duration) bright radio pulse from a decomissioned LEO satellite was recently observed in the 700–1000 MHz band with ASKAP (C. W. James et al. 2025). We conducted a search for LEO satellites above the Green Bank horizon at the time of GBP 220718. Using historical two-line element data from the Space-Track repository (United States Space Command 2022), we reconstructed the distribution of LEOs and found none within 5° of the GBT boresight (Azimuth: 45.3°, Elevation: 77.5°). The closest LEO at the time of the event was COSMOS 1320, launched in 1981, at an angular separation of 7.2°, while the nearest Starlink satellite (STARLINK-3843, a version 1.5 spacecraft) was over 17° away. While Starlink V1.5 satellites are designed for Ku-band communication, they emit unintended electromagnetic radiation in the 110–188 MHz range (F. Di Vruno et al. 2023; D. Grigg, S.

[2]https://scipy.org/.

J. Tingay & M. Sokolowski 2025). Whether this leakage extends into *L* band remains uncharacterized. However, given that these satellites would be in the far field of the GBT at these frequencies (where the beam is well-defined and sidelobe response is significantly attenuated), and given the large angular separations observed here, we consider it unlikely that LEO satellites produced GBP 220718.

4.2.2 Search for repetitions

The narrow-band nature of our observation of GBP 220718, and the complexity of its pulses discussed further below, motivated a series of follow-up observations to confirm it as a source of astrophysical nature, determine its origin and whether it is a repeating source.

We followed up our initial observation of GBP 220 718 with the Lovell Telescope at the Jodrell Bank Observatory (JBO). We observed the position determined in Section 3.4 for a total of 8 h and found no significant bursts. These observations were taken on nine days over the span of four months, from 2023 October 8 to 2024 February 15. The bandwidth of the observation is 336 MHz ranging from 1396 to 1732 MHz. The RFI environment around JBO during our observations was not very clean. The majority of bursts we detected with our `heimdall` pipeline were narrow-band RFI and easily recognized. Given the width of the original detection (17 ms), a system temperature of 30 K, a gain of 1 K Jy^{-1}, and a S/N of 10, we should be able to detect bursts of at least 83 mJy. Our non-detection precludes any bursts of this flux or greater during our observations.

The field of view containing GBP 220 718 was observed by CHIME/FRB for a total of about 150 h with a median 95 per cent completeness threshold of 3.5 Jy ms (FRB Collaboration 2026). No pulses were detected from this source above this fluence limit.

4.2.3 Dispersion measure of the main pulse

As shown in Fig. 5, the narrow-band nature of GBP 220 718 leads to a large bow-tie feature in the DM-time plane that is consistent with a pulse with a DM of 145.5 cm^{-3} pc, substantially higher than the Galactic contribution predicted by NE2025 (S. K. Ocker & J. M. Cordes 2026) or YWM16 (J. M. Yao, R. N. Manchester & N. Wang 2017) which predict DMs of 55.2 and 71.9 cm^{-3} pc, respectively. It is possible that GBP 220 718 is actually within the Milky Way, and that the apparent DM excess is due to inaccuracies in Galactic DM models along the line of sight. We searched the ATNF catalogue for any pulsars with DMs exceeding the NE2025 maximum line-of-sight DM by 90.3 cm^{-3} pc or the YMW16 maximum line-of-sight DM by 73.6 cm^{-3} pc, the excesses seen from this FRB. For each model, <1 per cent of pulsars showed such large excesses, making this an unlikely explanation. In fact, most of that group of pulsars lie in globular clusters or the Magellanic Clouds, which explain many of the discrepancies. Additionally, pulsars near GBP 220 718 in the sky do not appear to have anomalously high DMs, and the DM of GBP 220 718 is at least four times that of every known pulsar within 10 deg of its sky position.

If GBP 220 718 is astrophysical, we note that it is spatially coincident with the galaxy LEDA 2277 498 (G. Paturel et al. 2003). This candidate host, also identified as SDSS J072513.14+463143.5, lies at an angular separation of approximately 17″ from our best-fitting position, well within the estimated 1σ uncertainty. The galaxy is a faint dwarf system with a photometric redshift of $z_{\rm phot} \approx 0.082$ (R. Ahumada et al. 2020). The extragalactic DM (DM$_{\rm ext}$) of the burst further supports this association. While a crude DM$_{\rm ext} \sim 1000z$ scaling (E. Petroff, J. W. T. Hessels & D. R. Lorimer 2019) suggests $z \sim 0.07$, a more rigorous accounting of the foreground is required. In the direction of GBP 220 718 ($l = 176.3^\circ$, $b = 23.4^\circ$), the NE2025 model predicts a Galactic disc contribution of DM$_{\rm ISM} = 38$ cm^{-3} pc. Accounting for a halo contribution of $\sim$32 pc cm^{-3} (S. Yamasaki & T. Totani 2020) and an expected IGM contribution of DM$_{\rm IGM} \approx 66$ cm^{-3} pc at $z = 0.082$ (J.-P. Macquart et al. 2020), the observed DM is broadly consistent with an origin in LEDA 2277498. While these model-dependent subtractions suggest a low host contribution (DM$_{\rm host} \lesssim 30$ cm^{-3} pc), the large uncertainties in the halo and IGM components preclude a precise measurement. Nevertheless, the alignment in DM-space supports the possibility that the progenitor is located in a low-density environment, perhaps in the outskirts of the galaxy.

4.2.4 Scintillation analysis of the main pulse

If GBP 220 718 is astrophysical, it might display other effects of propagation through the interstellar and intergalactic mediums. Chief among these is diffractive scintillation, arising from inhomogeneities in the interstellar medium. Diffractive scintillation can be quantified by the diffractive time-scale $\Delta t_{\rm d}$ and diffractive bandwidth $\Delta \nu_{\rm d}$. These quantities can be estimated by computing the two-dimensional autocorrelation function (ACF) of the pulse's dynamic spectrum and averaging over frequency and time, respectively, then fitting each one-dimensional ACF to a Gaussian or Lorentzian function and measuring the widths of the fitted functions (J. M. Cordes, J. M. Weisberg & V. Boriakoff 1985; J. M. Cordes 1986). In particular, ν_d is calculated as the half width at half maximum of the fitted Gaussian or Lorentzian.

Efforts have been made to estimate $\Delta \nu_{\rm d}$ from observable quantities. N. D. R. Bhat et al. (2004) fit a relation between the scattering time-scale $\tau_{\rm s}$, DM and observing frequency f:

$$\log \tau_{\rm s} = -6.46 + 0.154 \log({\rm DM}) + 1.05(\log {\rm DM})^2 - 3.86 \log f, \quad (2)$$

where $\tau_{\rm s}$ is in milliseconds, DM is in cm^{-3} pc and f is in GHz. Assuming a DM of 145.5 cm^{-3} pc and a central observing frequency of 1.110 GHz, we find an expected scattering time-scale for GBP 220 718 of approximately 0.05 ms. For a Kolmogorov spectrum,

$$\Delta \nu_{\rm d} = \frac{1.16}{2\pi \tau_{\rm s}} \quad (3)$$

yielding an expected diffractive bandwidth of approximately 0.366 kHz. Unfortunately, this is significantly lower than the GREENBURST frequency channel bandwidth of 234 kHz, indicating that measuring $\Delta \nu_{\rm d}$ for GBP 220 718 may not be possible.

Given that there is a significant amount of scatter in the observed DM–$\tau_{\rm s}$ relation, we still attempt to measure a diffractive bandwidth for GBP 220718. We isolated the three largest features in the dynamic spectrum of the FRB, computed the one-dimensional frequency ACF for each subburst by averaging the two-dimensional ACF in time, and fit Lorentzians to each ACF, as the ACFs display strong wings. We arrived at measurements of

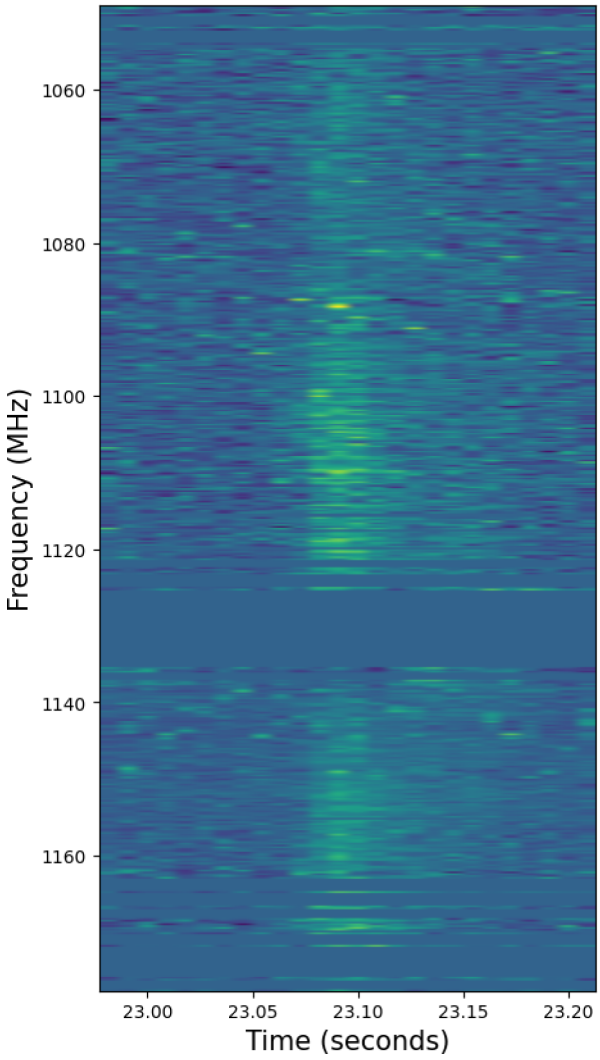

Figure 9. Dynamic spectrum of the main pulse of GBP 220718. Channels on the outside of the band were excised and not used to compute the ACF.

$\Delta\nu_d$ of 11 ± 4, 7.4 ± 2.5, and 7.9 ± 2.8 MHz, respectively. As an example, Fig. 9 shows the dynamic spectrum of the second of the three components used.

All three fits have difficulty fitting the central portion of the ACF, and so these widths are likely overestimates of the true diffractive bandwidth. Even accounting for this, the results are significantly higher than expected by the N. D. R. Bhat et al. (2004) relation. A closer examination of the dynamic spectra of the subbursts suggests that the fits may be absorbing spectral features of the burst, rather than actual diffractive scintillation.

4.2.5 Associated emission around the main pulse

Each time a significant pulse like GBP 220 718 is recorded, a filterbank file corresponding to the entire block of data (9 min) around that event is archived for offline analysis. Our examination of the data around GBP 220 718 does reveal other bursts of emission in this same band, as shown in Fig. 10. In addition to the bright central pulse, Fig. 10 shows several less luminous components that were present during the time the source was in the field of view of the telescope (≈40 s), but not initially detected by our real-time pipeline. As Fig. 10 shows, pulses are detected in three main regions of the time series which we label A, B, and C. Also shown are waterfall plots which show the frequency structure in these three regions. In this display, only the 100 MHz band in which GBP 220 718 was detected (Fig. 5) is shown and all data are de-dispersed to a DM of 145.5 cm^{-3} pc. Some of these components have similar spacing in time, especially in region B (where the main pulse was initially detected) and the spacing is approximately 0.85 s. A periodicity analysis on the data collected for the time series shown in Fig. 10, as well as region B alone using PRESTO (S. Ransom 2011) and RIPTIDE (V. Morello et al. 2020) did not yield any significant periodicities.

As Fig. 10 shows, while there clearly are other pulses present in the observation at the same DM of GBP 220718, there are a number of features in the same narrow frequency band that are consistent with DMs of zero. Such features are most prominent in region A which also shows a number of vertical bands (i.e. DM values around 145.5 cm^{-3} pc) alongside sloping features that correspond to sub-pulses consistent with zero DM. While a variation of slopes in multicomponent FRBs have been seen in CHIME/FRB data and described in detail in J. T. Faber et al. (2024), the features we observe in Fig. 10 show a much greater variation in DM over a much narrower band than seen by CHIME/FRB. If the emission shown here is truly astrophysical in nature, it would be unlike any other pulses seen to date.

While the initial pulse seen for GBP 220 718 shows a number of FRB-like properties, the presence of the additional pulses shown in Fig. 10, many of which exhibit no dispersion, while still falling in the same narrow frequency range, leads us to be skeptical of an astrophysical origin for this source. On the other hand, the fact that it passed our RFI filtering described in Section 2, which flags signals that are highly non-Gaussian means that we cannot safely conclude a terrestrial origin for the signal. The kurtosis and skew values for raw and RFI-filtered dynamic spectra are shown in Fig. 11. Emission from GBP 220 718 is visible in both intensity data, but without any corresponding increase in either kurtosis or skew. This is in contrast to the RFI bands visible in the left hand side, which show brightly in kurtosis and skew. In the absence of further information that would possible from an array receiver, we cannot currently rule out from this single-beam observation of GBP 220 718 with GREENBURST whether signal is terrestrial in nature. Our experiences with GBP 220 718 are consistent with the difficulties in classifying FRBs as discussed by G. Foster et al. (2018b).

5 CONCLUSIONS

The first 20 000 h of GREENBURST observations resulted in the detections of 50 pulsars, one of which (PSR J0039+5407) was previously unknown, three previously known FRBs and one dispersed pulse of unknown origin (GBP 220718). PSR J0039+5407 is a 2.2 s pulsar with a nulling fraction on the order of 80 per cent. GBP 220 718 was originally detected as a narrow-band signal with a DM of 145.5 cm^{-3} pc. Based on FRB observations to date, such properties are consistent with a nearby repeating FRB. However, in spite of significant follow-up observations with other telescopes, no additional events were found. In addition, upon closer inspection of the data taken around the epoch of detection for GBP 220718, however, we found a number of additional pulses that are consistent with zero DM signals in the same part of the band. We searched for possible LEO satellites above the horizon at the time of the observation of GBP 220718, but found none. In

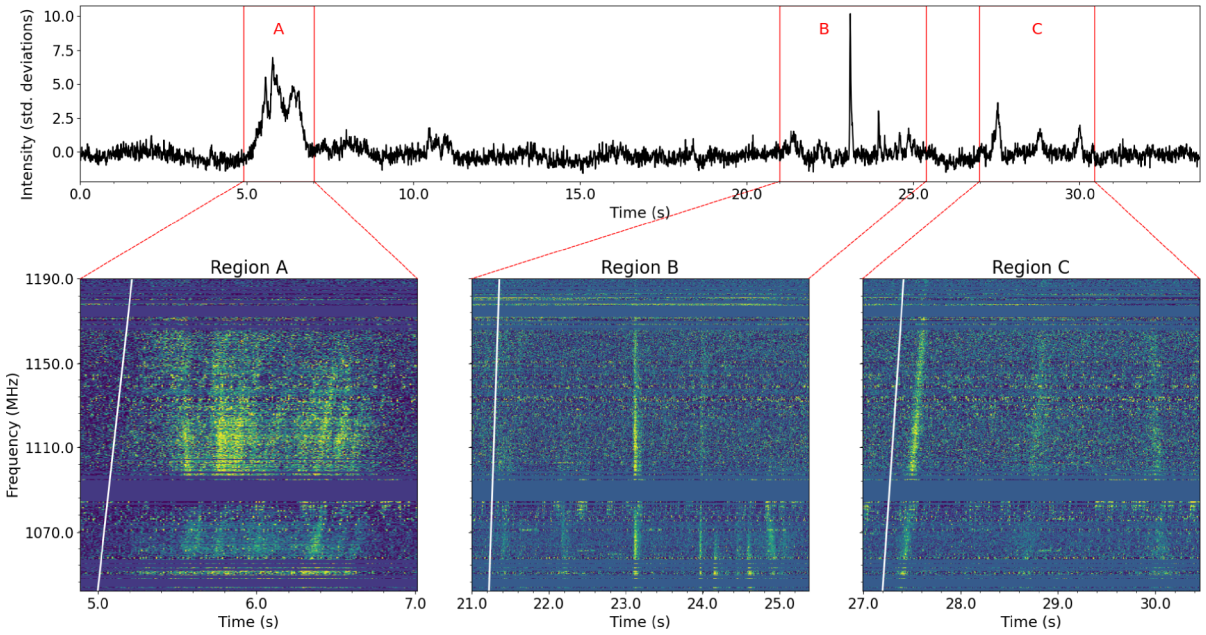

Figure 10. Summary of the observation containing all the emission recorded from GBP 220718, cleaned with the composite filter described in (J. W. Kania et al. 2026) with weighted zero-DM subtraction. The top panel shows the dedispersed time series referenced to a DM of 145.5 cm^{-3} pc. Three different regions are shown, referred to as A, B, and C. The bottom panels show waterfall plots also dedispersed to a DM of 145.5 cm^{-3} pc zooming in around each region. The original detection shown in Fig. 5 is the bright pulse at the centre of region B. The white lines show the expected behaviour for a zero-DM signal.

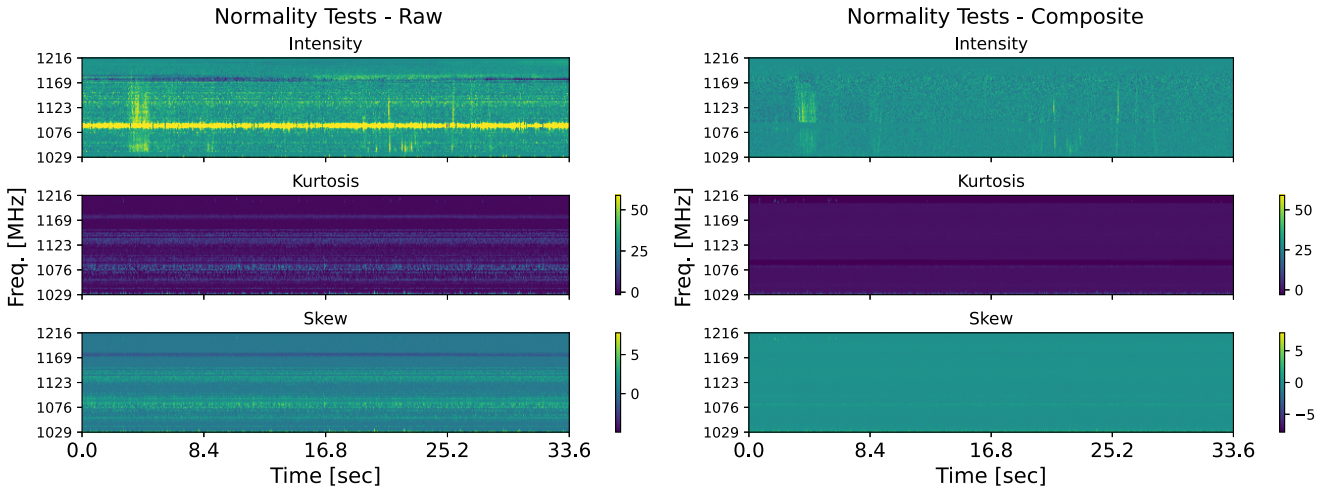

Figure 11. Kurtosis and skew analyses on blocks of 64 times samples for the data containing GBP 220718. The left hand plots show the data without any RFI filtering, the right hand plots are post cleaning with the composite filter (J. W. Kania et al. 2026) with weighted zero-DM subtraction. For both cases, we show the dynamic spectra (top), kurtosis values (middle), and skew values (bottom). As the right-hand panels show, there is no significant kurtosis or skew for GBP 220718.

addition, the higher order moments of GBP 220 718 are inconsistent with most known sources of terrestrial origin. If astrophysical, GBP 220 718 appears to be coincident with the nearby galaxy LEDA 2277498. Further observations are necessary to make a firm conclusion as to whether GBP 220 718 is astrophysical or terrestrial in nature.

GREENBURST observations currently underway include a single-pulse study of all the millisecond pulsars we have observed to date (Tabassum et al. in preparation) and a survey of nearby elliptical galaxies for FRBs (Paine et al. in preparation). Ongoing work is focused on extending the range of pulse widths searched to improve the sensitivity of GREENBURST to long-period transients (see, e.g. N. Hurley-Walker et al. 2023), providing sensitivity to events such as the one seen in region A of Fig. 10.

ACKNOWLEDGEMENTS

The Green Bank Observatory is a facility of the National Science Foundation (NSF) operated under cooperative agreement by Associated Universities, Inc. We thank Green Bank Observatory staff Ryan Lynch and Evan Smith for their assistance

with the followup observations. GREENBURST operations have been supported by NSF Astrononomy and Astrophysics awards 1616042 and 2406570. SP and DRL acknowledge support from NSF award 2406570. ST and DRL acknowledge support from NSF award 2307581. SS and KEH are WVU Ruby Doctoral Fellows. MF acknowledges support from the WV Spacegrant Consortium. EJM acknowledges NSF support from the WVU Research Experiences for Undergraduates programme under award 2348764. FAD is supported by an National Radio Astronomy Observatory Jansky Fellowship. We acknowledge that CHIME is located on the traditional, ancestral, and unceded territory of the Syilx/Okanagan people. We are grateful to the staff of the Dominion Radio Astrophysical Observatory, which is operated by the National Research Council of Canada. CHIME operations are funded by a grant from the NSERC Alliance Programme and by support from McGill University, University of British Columbia, and University of Toronto. CHIME was funded by a grant from the Canada Foundation for Innovation (CFI) 2012 Leading Edge Fund (Project 31170) and by contributions from the provinces of British Columbia, Québec and Ontario. The CHIME/FRB Project, which enabled development in common with the CHIME/Pulsar instrument, was funded by a grant from the CFI 2015 Innovation Fund (Project 33213) and by contributions from the provinces of British Columbia and Québec, and by the Dunlap Institute for Astronomy and Astrophysics at the University of Toronto. Additional support was provided by the Canadian Institute for Advanced Research (CIFAR), the Trottier Space Institute at McGill University, and the University of British Columbia. The CHIME/Pulsar instrument hardware is funded by the Natural Sciences and Engineering Research Council (NSERC) Research Tools and Instruments (RTI-1) grant EQPEQ 458893–2014. We thank Matthew Stevenson for assistance with the LEO satellite analysis and the referee for very useful comments on an earlier version of the manuscript.

DATA AVAILABILITY

All GREENBURST triggers are available from the authors upon reasonable request. Processed data from the pipeline for detections of known pulsars are available via the GREENBURST website: https://greenburstwvu.github.io.

REFERENCES

Agarwal D., 2020, PhD thesis, West Virginia Univ., https://researchrepository.wvu.edu/etd/7827
Agarwal D. et al., 2020a, MNRAS, 497, 352
Agarwal D., Aggarwal K., Burke-Spolaor S., Lorimer D. R., Garver-Daniels N., 2020b, MNRAS, 497, 1661
Ahumada R. et al., 2020, ApJS, 249, 3
Archer K., Siemion A., Werthimer D., Lebofsky M., Cobb J., Abdurashidova Z., Hickish J., 2016, United States National Committee of URSI National Radio Science Meeting (USNC-URSI NRSM). Boulder, CO, USA. p. 1
Backer D. C., 1970, Nature, 228, 42
Barsdell B. R., 2012, PhD thesis, Swinburne Univ. Technol., Australia
Bera A. K., Jarque C. M., 1981, Econ. Lett., 7, 313
Bhardwaj M. et al., 2021, ApJ, 910, L18
Bhat N. D. R., Cordes J. M., Camilo F., Nice D. J., Lorimer D. R., 2004, ApJ, 605, 759
Biggs J. D., 1992, ApJ, 394, 574
Bilous A. V., Ransom S. M., Demorest P., 2019, ApJ, 877, 125
Bochenek C. D., Ravi V., Belov K. V., Hallinan G., Kocz J., Kulkarni S. R., McKenna D. L., 2020, Nature, 587, 59
Brook P. R., Karastergiou A., Johnston S., 2019, MNRAS, 488, 5702
Burgay M. et al., 2003, Nature, 426, 531
Burke-Spolaor S. et al., 2012, MNRAS, 423, 1351
CHIME/FRB Collaboration, 2018, ApJ, 863, 48
CHIME/FRB Collaboration, 2019, Nature, 566, 235
CHIME/FRB Collaboration, 2020, Nature, 587, 54
CHIME/Pulsar Collaboration, 2021, ApJS, 255, 5
Caleb M. et al., 2025, preprint (arXiv:2508.01648)
Chennamangalam J. et al., 2017, ApJS, 228, 21
Cognard I., Shrauner J. A., Taylor J. H., Thorsett S. E., 1996, ApJ, 457, L81
Cordes J. M., 1986, ApJ, 311, 183
Cordes J. M., Weisberg J. M., Boriakoff V., 1985, ApJ, 288, 221
D'Agostino R., Pearson E. S., 1973, Biometrika, 60, 613
D'Agostino R. B., Belanger A., 1990, Am. Stat., 44, 316
Di Vruno F., Winkel B., Bassa C. G., Józsa G. I. G., Brentjens M. A., Jessner A., Garrington S., 2023, A&A, 676, A75
Eatough R. P., Keane E. F., Lyne A. G., 2009, MNRAS, 395, 410
FRB Collaboration, 2026, preprint (arXiv:2601.09399)
Faber J. T. et al., 2024, ApJ, 974, 274
Foster G. et al., 2018a, MNRAS, 474, 3847
Foster G. et al., 2018b, MNRAS, 481, 2612
Gary D. E., Liu Z., Nita G. M., 2010, PASP, 122, 560
Golpayegani G., 2020, PhD thesis, West Virginia Univ., https://researchrepository.wvu.edu/etd/7545
Grigg D., Tingay S. J., Sokolowski M., 2025, A&A, 699, A307
Hobbs G. B., Edwards R. T., Manchester R. N., 2006, MNRAS, 369, 655
Hurley-Walker N. et al., 2023, Nature, 619, 487
James C. W. et al., 2025, ApJ, 987, L16
Jarque C. M., Bera A. K., 1980, Econ. Lett., 6, 255
Jarque C. M., Bera A. K., 1987, Int. Stat. Rev./Rev. Int. Stat., 55, 163
Kania J. W., 2023, PhD thesis, West Virginia Univ., https://researchrepository.wvu.edu/etd/12243
Kania J. W., Bandura K., Lorimer D. R., Prestage R., 2026, ApJ, 171, 73
Lazarus P. et al., 2015, ApJ, 812, 81
Lorimer D. R., 2011, Astrophysics Source Code Library, record ascl:1107.016
Lorimer D. R., Kramer M., 2004, Handbook of Pulsar Astronomy, Vol 4. Cambridge Univ. Press, Cambridge
Lyne A. G. et al., 2004, Science, 303, 1153
Macquart J.-P. et al., 2020, Nature, 581, 391
McDowell J. C., 2020, ApJ, 892, L36
Mickaliger M. B., McEwen A. E., McLaughlin M. A., Lorimer D. R., 2018, MNRAS, 479, 5413
Mirhosseini A., 2020, PhD thesis, Univ. British Columbia, https://open.library.ubc.ca/collections/ubctheses/24/items/1.0394838
Morello V., Barr E. D., Stappers B. W., Keane E. F., Lyne A. G., 2020, MNRAS, 497, 4654
Morello V., Rajwade K. M., Stappers B. W., 2022, MNRAS, 510, 1393
Nita G. M., Gary D. E., 2010, PASP, 122, 595
Nita G. M., Gary D. E., Liu Z., Hurford G. J., White S. M., 2007, PASP, 119, 805
Nita G. M., Keimpema A., Paragi Z., 2019, J. Astron. Instrum., 08, 1940008
Niu C. H. et al., 2022, Nature, 606, 873
Ocker S. K., Cordes J. M., 2026, preprint (arXiv:2602.11838)
Parzen E., 1962, Ann. Math. Stat., 33, 1065
Paturel G., Petit C., Prugniel P., Theureau G., Rousseau J., Brouty M., Dubois P., Cambrésy L., 2003, A&A, 412, 45
Pedregosa F. et al., 2011, J. Mach. Learn. Res., 12, 2825
Petroff E., Hessels J. W. T., Lorimer D. R., 2019, A&AR, 27, 4
Platts E., Weltman A., Walters A., Tendulkar S. P., Gordin J. E. B., Kandhai S., 2019, Phys. Rep., 821, 1
Prestage R. M. et al., 2015, URSI-USNC Radio Science Meeting. Boulder, CO, USA. p. 4
Rafiei-Ravandi M., Smith K. M., 2023, ApJS, 265, 62
Ransom S., 2011, Astrophysics Source Code Library, record ascl:1107.017
Ritchings R. T., 1976, MNRAS, 176, 249

Rosenblatt M., 1956, Ann. Math. Stat., 27, 832
Rousseeuw P., Croux C., 1992, in Dodge Y., Whittaker J., Computational Statistics. Vol. 1, Physica-Verlag, Heidelberg, p. 411
Ryder S. D. et al., 2023, Science, 382, 294
Smith E., Lynch R. S., Pisano D. J., 2022, AJ, 164, 123
Spitler L. G. et al., 2016, Nature, 531, 202
Surnis M. P. et al., 2019, Publ. Astron. Soc. Aust., 36, e032
Taylor J., Denman N., Bandura K., Berger P., Masui K., Renard A., Tretyakov I., Vanderlinde K., 2019, J. Astron. Instrum., 08, 1940004
United States Space Command, 2022, Space-Track.org, https://www.space-track.org
Virtanen P. et al., 2020, Nat. Methods, 17, 261
Wang N., Manchester R. N., Johnston S., 2007, MNRAS, 377, 1383
Yamasaki S., Totani T., 2020, ApJ, 888, 105
Yao J. M., Manchester R. N., Wang N., 2017, ApJ, 835, 29
Zhang B., 2023, Rev. Mod. Phys., 95, 035005

This paper has been typeset from a TEX/LATEX file prepared by the author.